Electronic Supplementary Material (ESI)

Ultrasmall diiron phosphide nanodots anchored on graphene sheets with enhanced electrocatalytic activity for hydrogen production via high-efficiency water splitting

Huawei Huang, Chang Yu, Juan Yang, Xiaotong Han, Changtai Zhao, Shaofeng Li, Zhibin Liu and Jieshan Qiu*

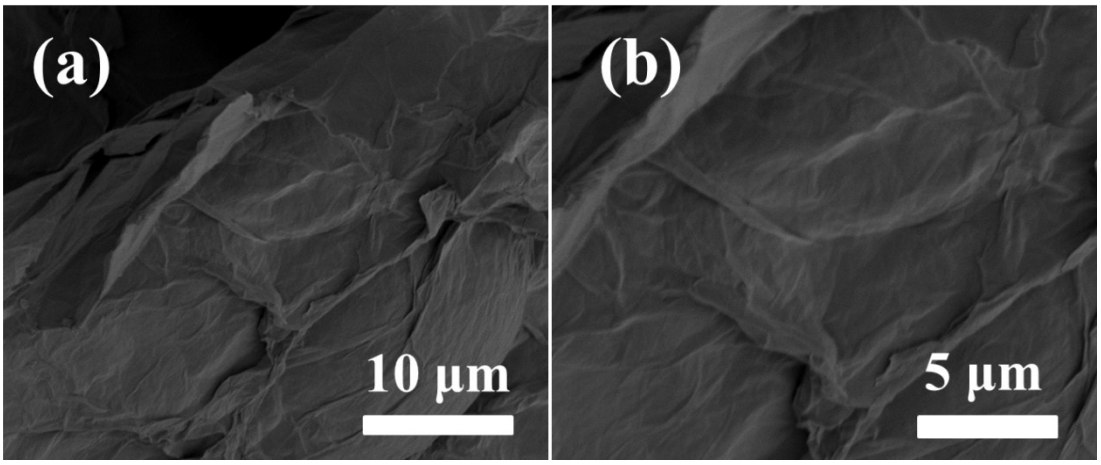

Fig. S1 FE-SEM images of the as-made GO.

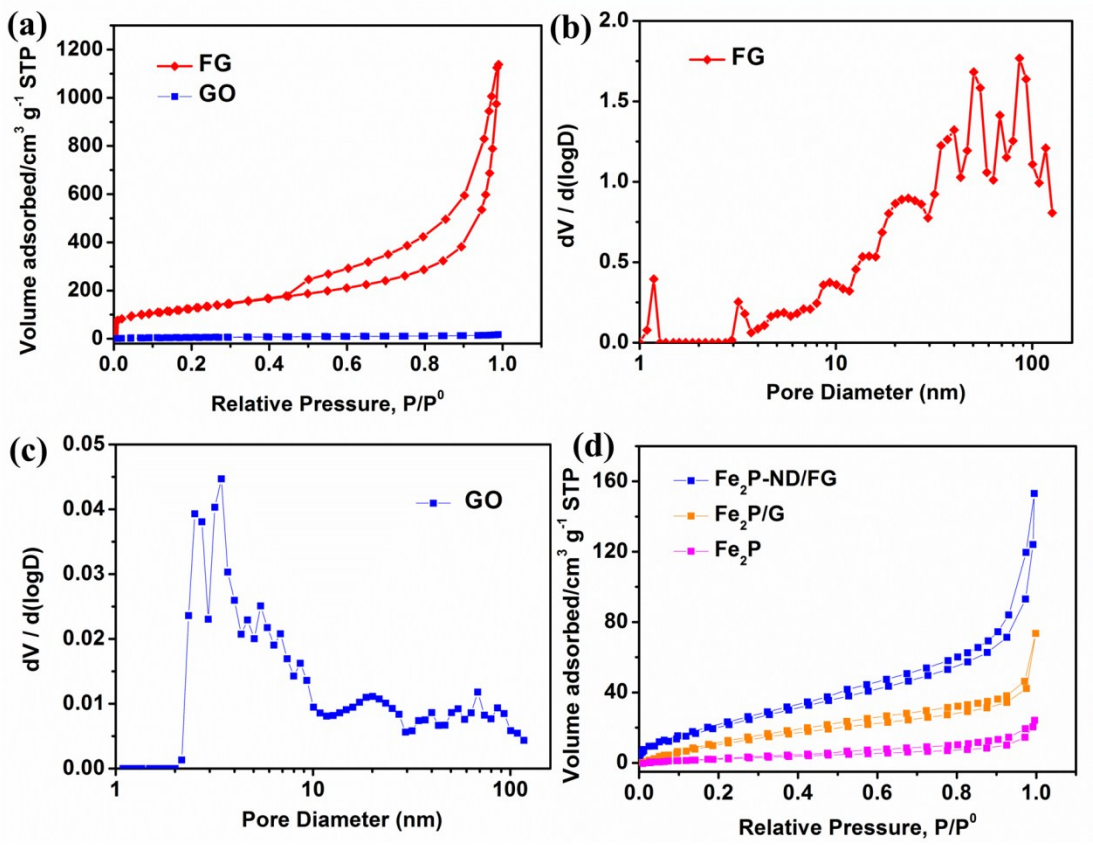

Fig. S2 a) Nitrogen adsorption-desorption isotherms and b, c) pore-size distribution curves of the as-made FG, GO; d) Nitrogen adsorption-desorption isotherms of Fe_2P-ND/FG, Fe_2P/G, and Fe_2P.

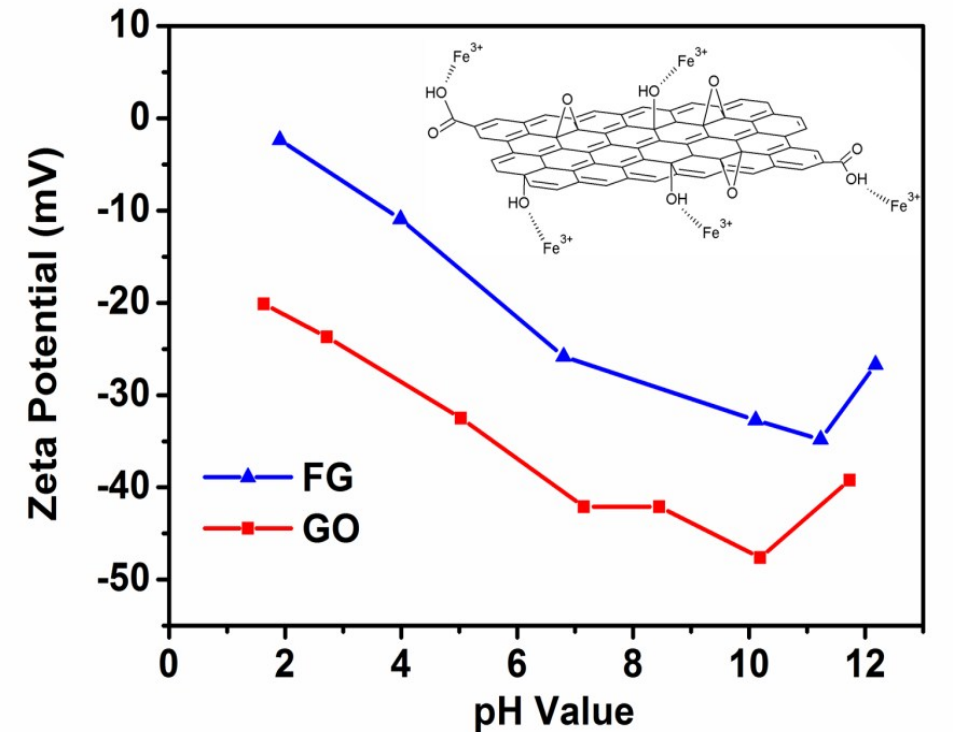

Fig. S3 Zeta potentials of FG and GO at different pH values (inset: schematic for ferric ions adsorbed on the FG surface).

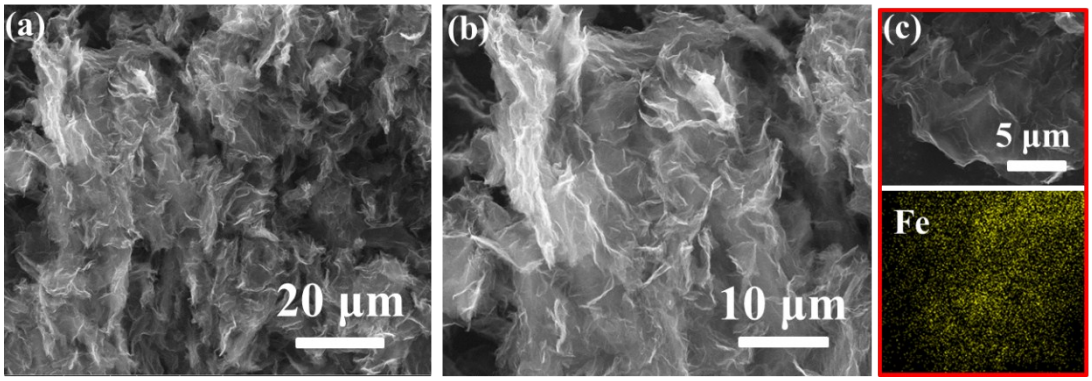

Fig. S4 a, b) FE-SEM images of Fe_2O_3-ND/FG; c) FE-SEM image of Fe_2O_3-ND/FG and corresponding EDX elemental mapping of Fe.

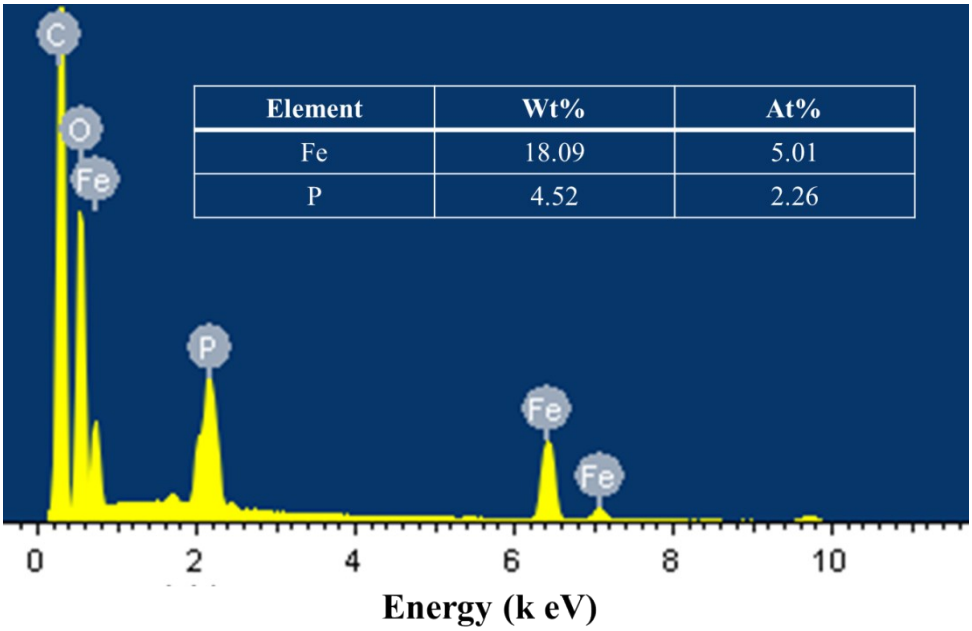

Element	Wt%	At%
Fe	18.09	5.01
P	4.52	2.26

Fig. S5 EDX spectrum of the as-made Fe_2P-ND/FG hybrids.

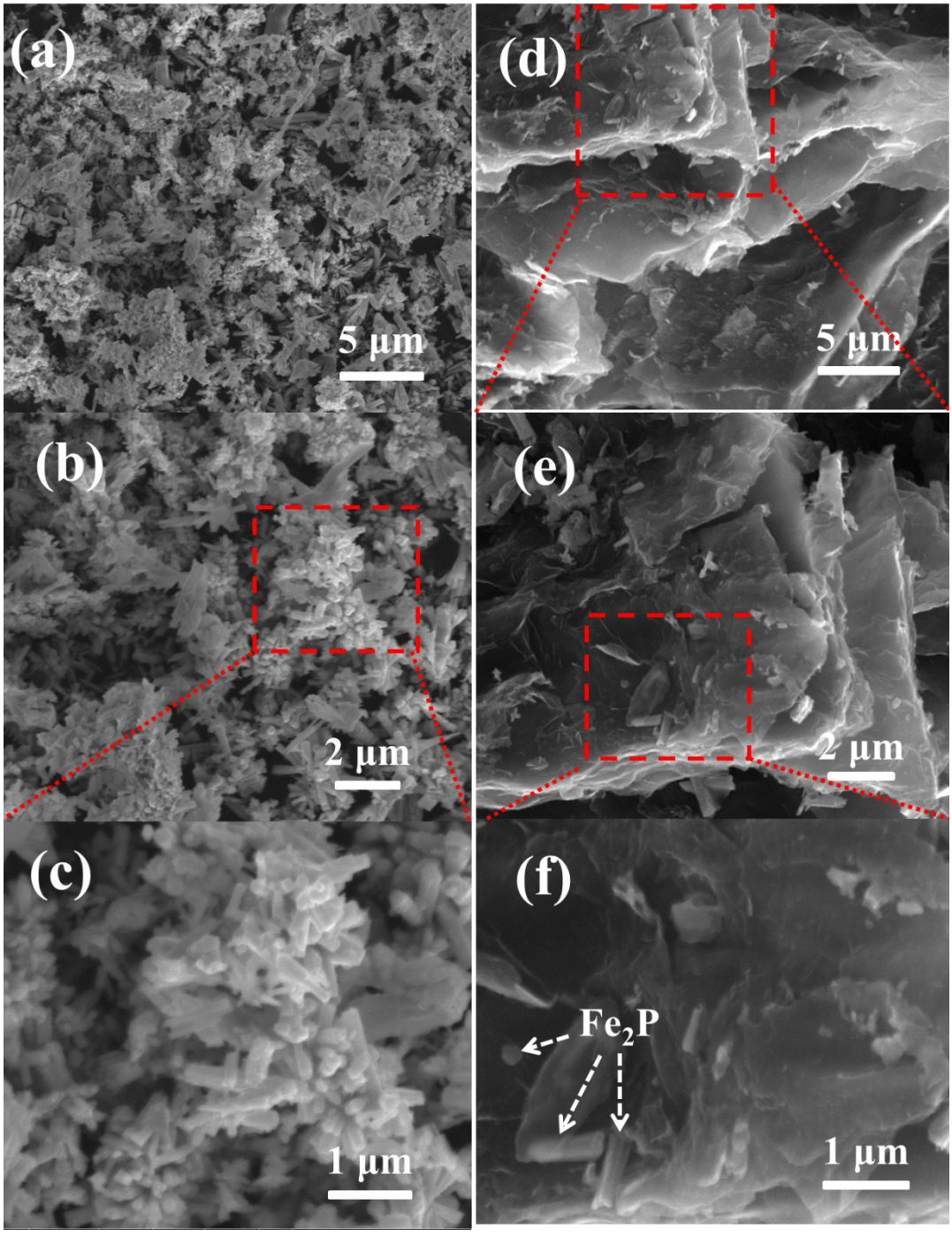

Fig. S6 FE-SEM images of a-c) the pure Fe_2P and d-f) Fe_2P/G.

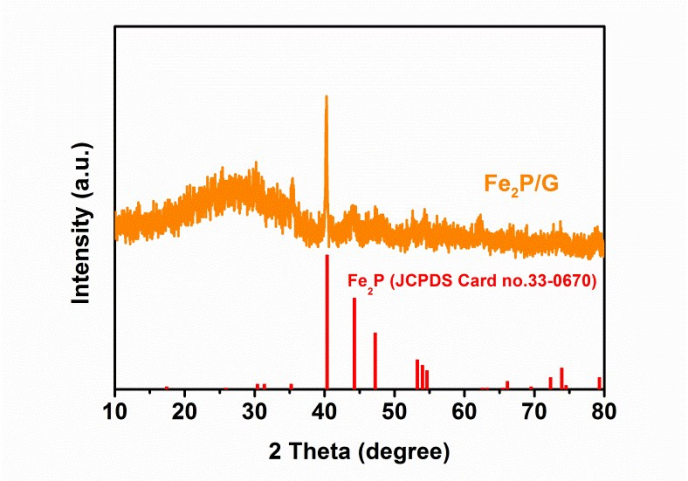

Fig. S7 XRD patterns of Fe_2P/G and standard Fe_2P (JCPDS Card no. 33-0670).

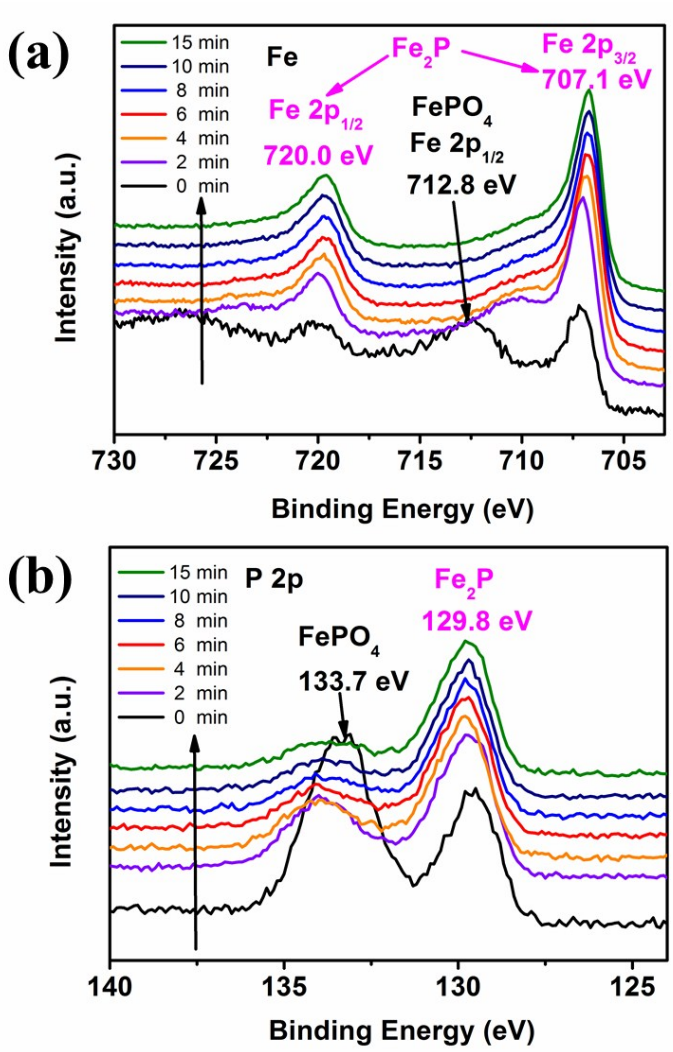

Fig. S8 Depth XPS spectra of a) Fe 2p and b) P 2p regions for Fe_2P after 0-, 2-, 4-, 6-, 8-, 10-, and 15-min Ar ion etching.

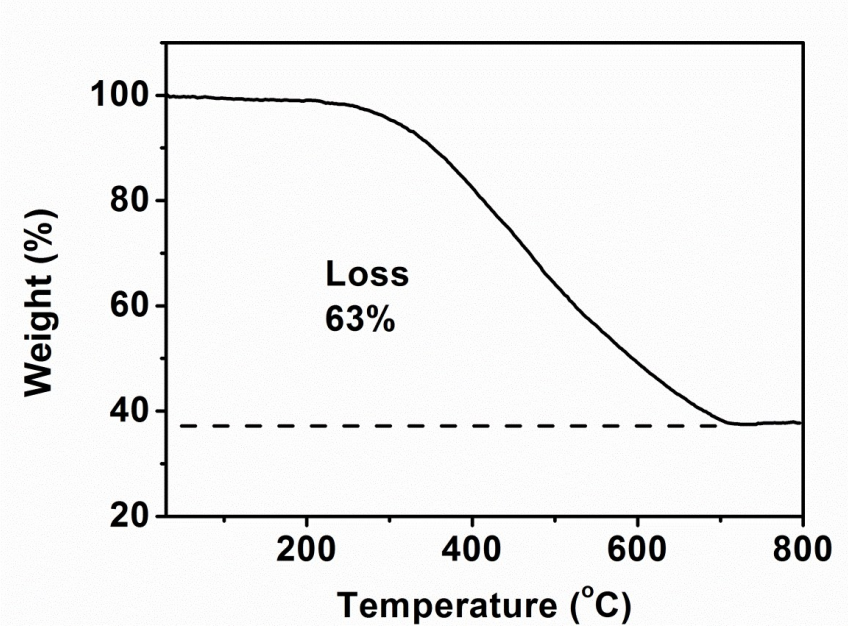

Fig. S9 TGA curve of the Fe_2O_3/FG.

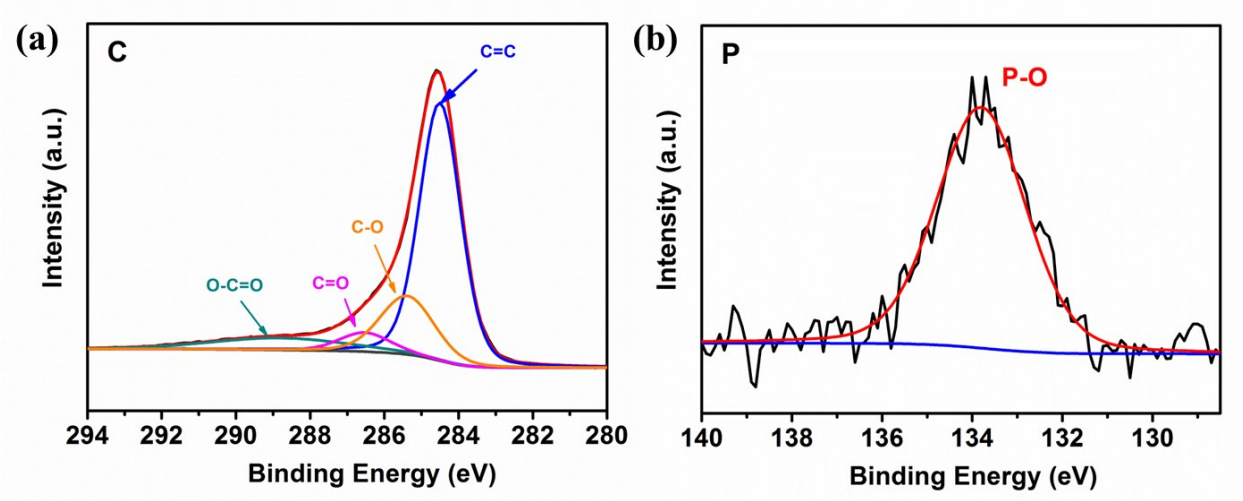

Fig. S10 XPS spectra of a) C 1s and b) P 2p for the as-made FG-P.

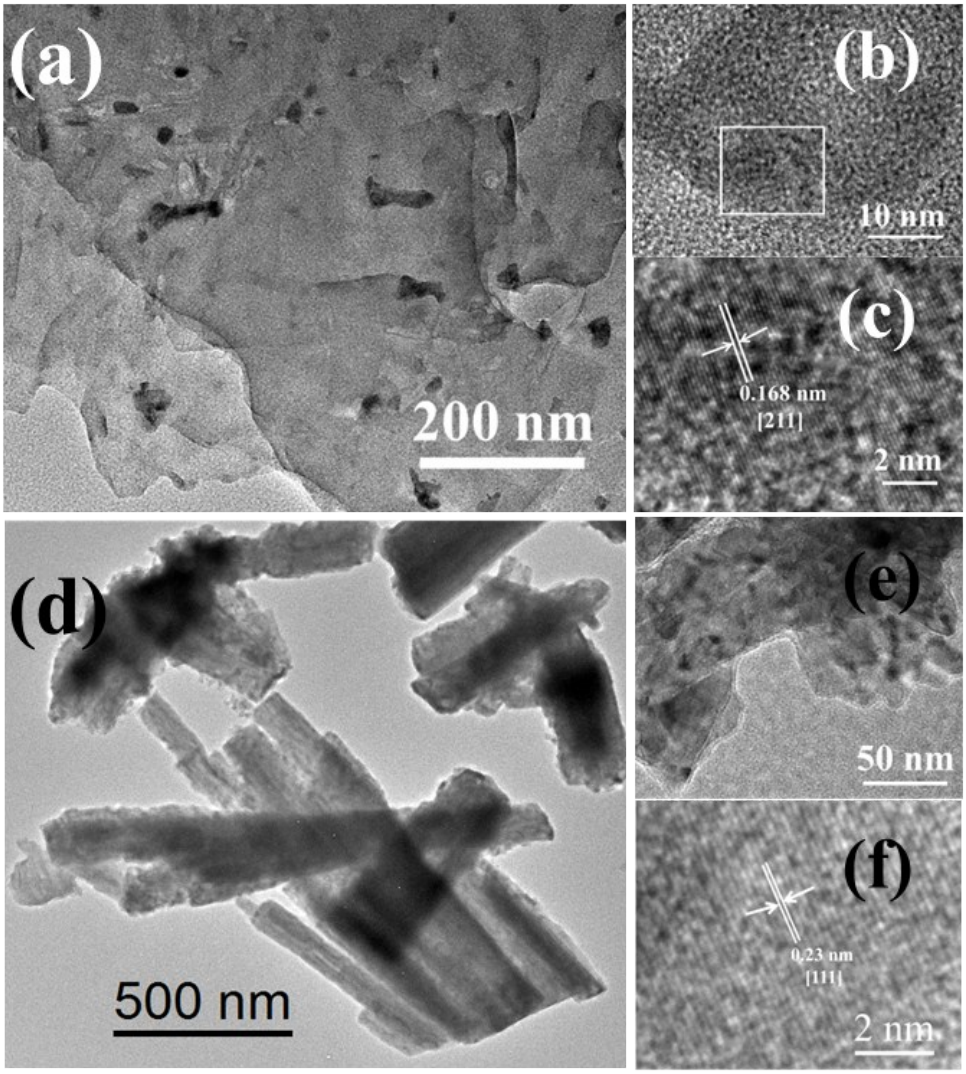

Fig. S11 The morphology of the as-prepared samples: a, b) TEM and c) HR-TEM images of the Fe_2P/G composites; d, e) TEM and f) HR-TEM images of pure Fe_2P.

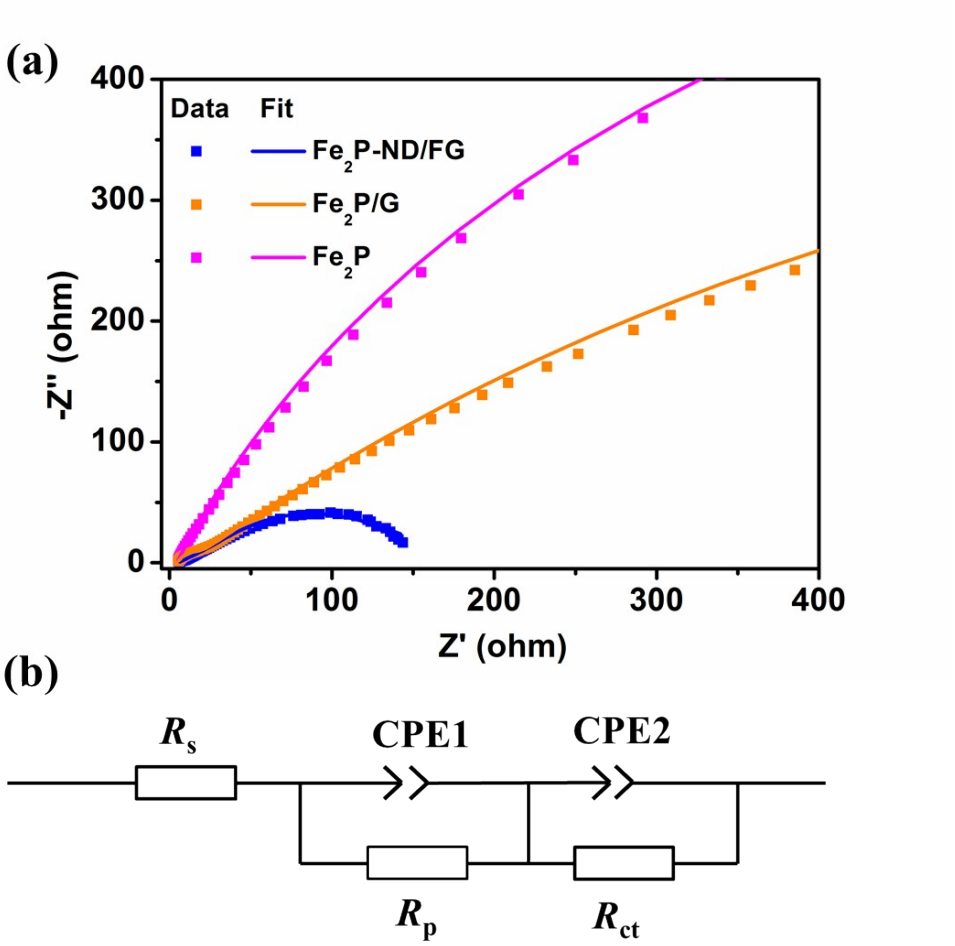

Fig. S12 a) Nyquist plots of the as-made Fe_2P, Fe_2P/G and Fe_2P-ND/FG at an overpotential -150 mV versus RHE. The square symbols are experimental data and line is modeled by equivalent electrical circuit shown in b). b) Equivalent electrical circuit used to model the EIS data, consisting of a series resistance (R_s), two constant phase elements (CPE1 and CPE2), resistance related to surface porosity (R_p), and charge transfer resistance related to HER process (R_{ct}).

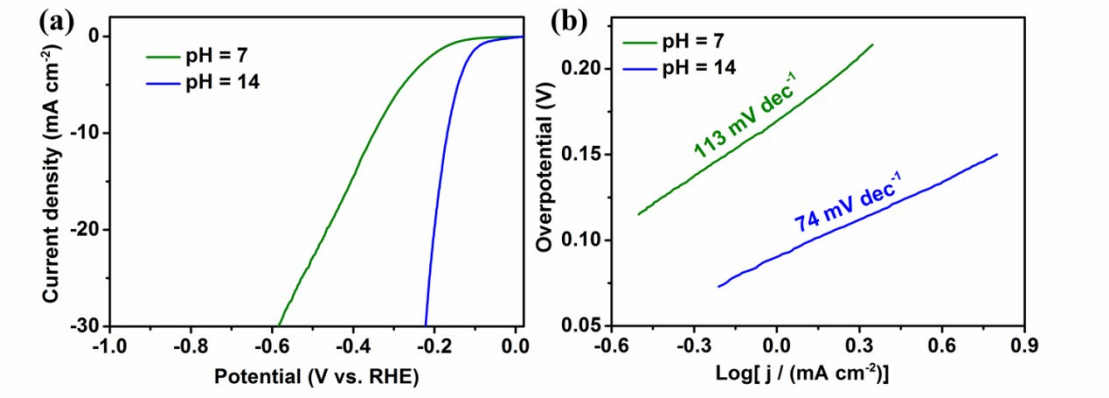

Fig. S13 a) Polarization curves and b) the corresponding Tafel plots for the as-made Fe_2P-ND/FG in 1 M KOH (pH=14) and 1 M PBS (pH=7).

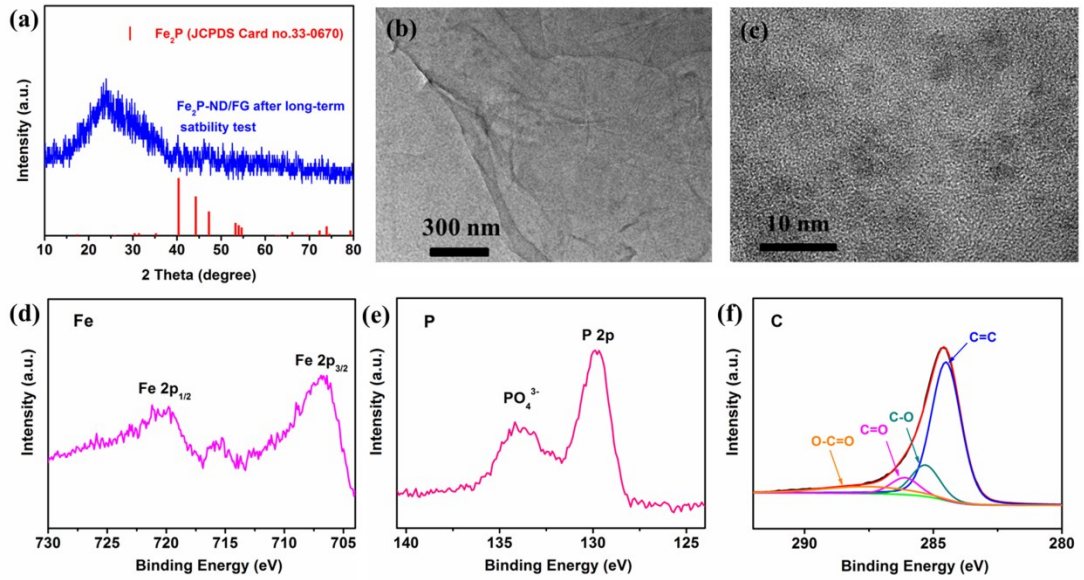

Fig. S14 a) XRD patterns, b-c) TEM images, d) Fe 2p, e) P 2p, and f) C 1s XPS spectra of Fe_2P-ND/FG after long term stability test.

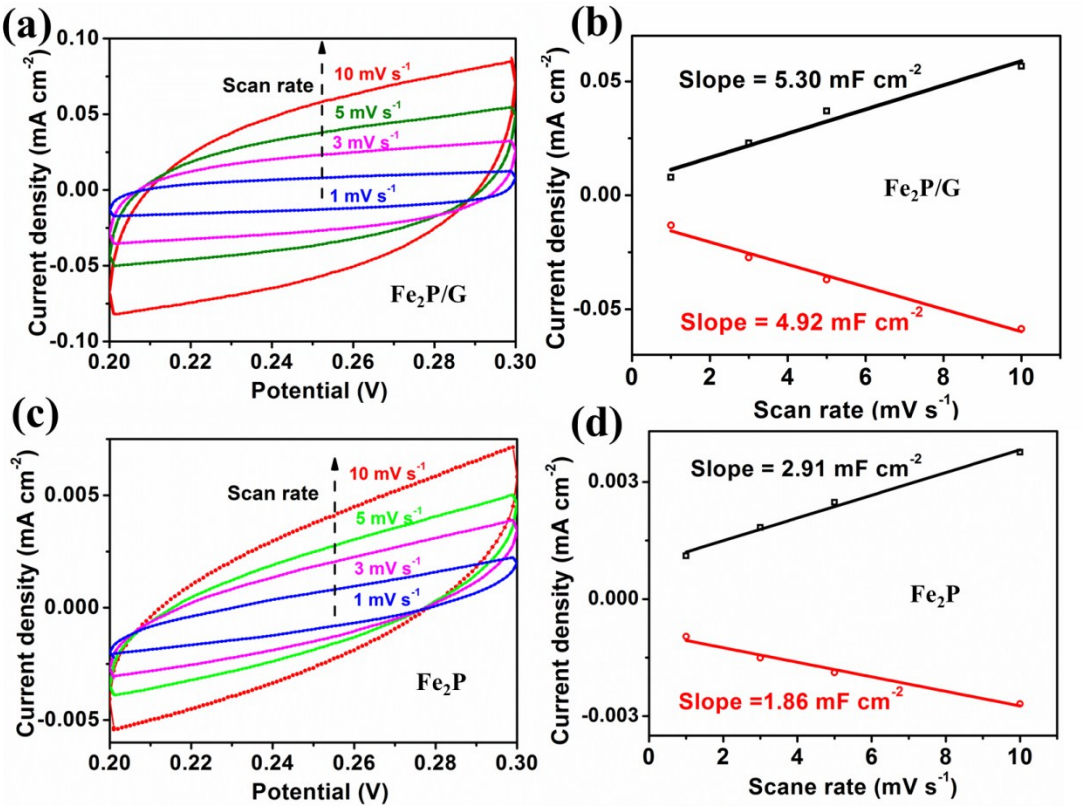

Fig. S15 Electrochemical double-layer capacitance of the as-made samples. a) and c) cyclic voltammograms of the as-made Fe_2P/G and Fe_2P at different scan rates in the no Faradaic potential range from 0.2 to 0.3 V vs. RHE; b) and d) the anodic (black line) and cathodic (red line) charging currents measured at 0.25 V vs. RHE, plotted against the scan rates. The double-layer capacitance of Fe_2P/G (5.11 mF cm^{-2}) and Fe_2P (2.59 mF cm^{-2}) determined from this system is taken by the average of the absolute value of anodic and cathodic slopes of the linear fits.

The calculation of electrochemical active surface area:

For the estimation of ECAS, a specific capacitance (C_s) value C_s = 40 μF cm^{-2} is adopted, which is commonly used in the literature and the ECAS of the as-made electrocatalysts is calculated according to $A_{ESCA} = C_{dl}/C_s$. [1] The detailed results are as follows:

Fe_2P-ND/FG:

$$A_{ECSA}^{Fe_2P/FG} = \frac{15.22\ mF\ cm^{-2}}{40\ \ \mu F\ cm^{-2}\ per\ cm_{ECSA}^{2}} = 380\ cm^2$$

Fe_2P/G:

$$A_{ECSA}^{Fe_2P/G} = \frac{5.11\ mF\ cm^{-2}}{40\ \ \mu F\ cm^{-2}\ per\ cm_{ECSA}^{2}} = 128\ cm_{ECSA}^{2}$$

Fe_2P:

$$A_{ECSA}^{Fe_2P} = \frac{2.59\ mF\ cm^{-2}}{40\ \ \mu F\ cm^{-2}\ per\ cm_{ECSA}^{2}} = 65\ cm_{ECSA}^{2}$$

TOF calculations:

The TOF values for the as-made samples are calculated by following the method in the literature [1, 2].To calculate the per-site TOF, the following formula is adopted [1]:

$$TOF = \frac{\#\ total\ hydrogen\ turn\ overs/cm^2\ geometricarea}{\#\ active\ sites/cm^2\ geometricarea}$$

The total number of hydrogen turn overs was calculated from the current density according to:

$$\#_{H_2} = \left(j\frac{mA}{cm^2}\right)\left(\frac{1C\ s^{-1}}{1000\ mA}\right)\left(\frac{1\ mol\ e^{-1}}{96485.3\ C}\right)\left(\frac{1\ mol\ H_2}{2\ mol\ e^{-1}}\right)\left(\frac{6.022\times10^{23}\ H_2\ molecules}{1\ mol\ H_2}\right)$$

$$= 3.12\times10^{15}\frac{H_2/s}{cm^2}\ per\ \frac{mA}{cm^2}$$

There are a number of possible binding sites for hydrogen on the TMPs, such as the hydrogen could adsorb onto a metal site, a phosphorous site, a bridge site between a metal and phosphorous, or other types of sites. Since the exact reaction mechanism of TMP for HER is not known, the number of surface sites including both Fe and P atoms derived from the roughness factor together with the unit cell (volume = 96.95 Å^3, see Fig. S16) is usually called as possible active sites, which is a widely used

approach for evaluating TOF value. [1, 2]

#active sites per real surface area:

$$\#active\ sites = \left(\frac{3\ atoms\ /unit\ cell}{96.95\text{Å}^3\ /unit\ cell}\right)^{\frac{2}{3}} = 9.856 \times 10^{14} atoms\ cm_{real}^{-2}$$

$$TOF = \frac{(3.12 \times 10^{15} \frac{H_2/s}{cm^2}\ per\ \frac{mA}{cm^2}) \times |j|}{(9.856 \times 10^{14} atoms\ cm_{real}^{-2}) \times A_{ECSA}}$$

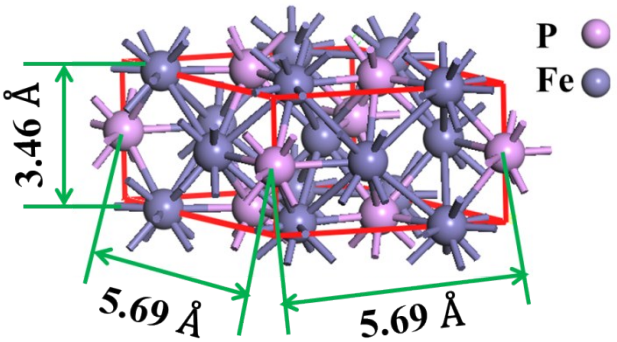

Fe_2P unit cell:
Volume: 96.95 Å^3
Contains: 2 Fe and 1 P atom

Fig. S16 The size of Fe_2P unit cell.

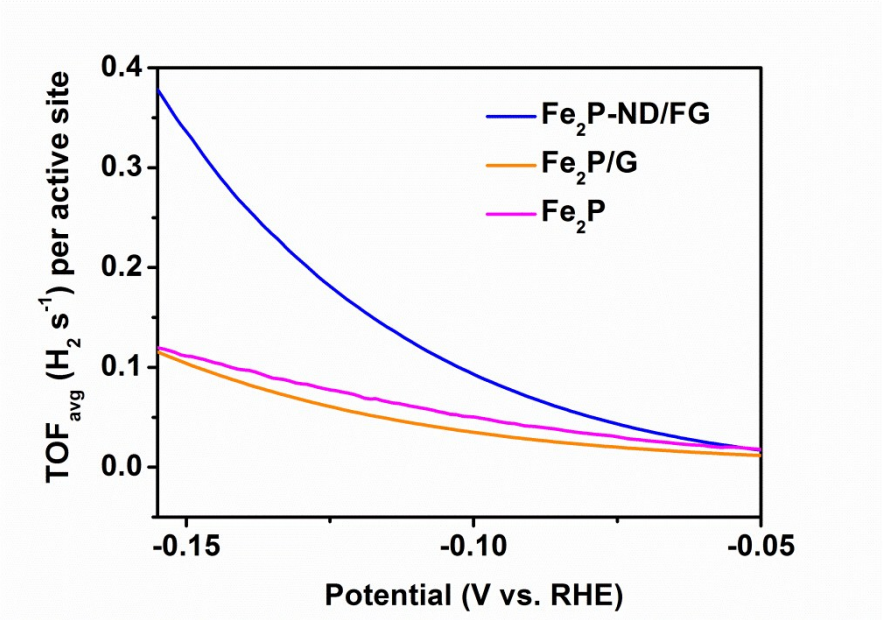

Fig. S17 TOF values of the as-made Fe_2P-ND/FG, Fe_2P/G, and Fe_2P at different overpotentials.

Table S1: Comparison of HER catalytic activity over different electrocatalysts.

Catalyst	Current density (j, mA cm^{-2})	η (mV) at the corresponding j	Tafel slope (mV dec^{-1})	Loading of catalyst (mg cm^{-2})	Ref.
Fe_2P-ND/FG	2	44	47	0.4	This work
	10	91			
	20	117			
Pt/C	2	16	30	0.4	This work
	10	36			
	20	52			
Ni_2P	20	130	46	1	**2**
CoP/CNT	2	70	54	0.285	**3**
	10	122			
MoS_2/RGO	onset	100	41	0.28	**4**
	10	150			
MoS_2 quantum dots	onset	120	69	NA	**5**
	10	250			
$Fe_{0.9}Co_{0.1}S_2$/CNT	onset	90	46	7	**6**
	20	120			
Ni_3FeN-NPs	10	158	42	0.35	**7**
Ni_5P_4-Ni_2P	1	54	79.1	NA	**8**
	10	120			
P-WN/RGO	10	85	54	0.337	**9**
Fe_2P/NGr	onset	60	65	1.71	**10**
	10	138			
Porous MoC_x	1	87	53	0.8	**11**
	10	142			
NiS	10	94	139	1	**12**
Co phosphide/phosphate	30	175	53	0.1	**13**
Pt NWs/SL-$Ni(OH)_2$	2.48	70	NA	0.16	**14**
$CoMoS_3$	1	112	56.9	0.5	**15**
	10	171			
Co-NRCNTs	1	140	80	0.28	**16**
	10	260			
MoS_2/RGO_2	onset	140	41	0.2	**17**
	20	200			
Cu_3P NW/CF	onset	62	67	15.2	**18**
	10	143			

Note: The definition of "onset potential" is vague, the authors have different criterions (overpotential attains current density from 0.1 to 1 mA cm^{-2}) [19, 20].

Table S2: BET surface area, exchange current density (j_0), and normalized j_0 of as-made electrocatalysts.

Catalysts	BET surface area ($m^2\ g^{-1}$)	j_0 ($A\ cm^{-2}$)	normalized j_0 ($A\ cm^{-2}{}_{BET}$)
Fe_2P-ND/FG	113	2.6×10^{-4}	5.8×10^{-8}
Fe_2P/G	51	1.4×10^{-4}	6.8×10^{-8}
Fe_2P	13	1.1×10^{-4}	2.1×10^{-7}

[1] J. Kibsgaard, T. F. Jaramillo, *Angew. Chem. Int. Ed.* **2014**, *53*, 14433.

[2] E. J. Popczun, J. R. McKone, C. G. Read, A. J. Biacchi, A. M. Wiltrout, N. S. Lewis, R. E. Schaak, *J. Am. Chem. Soc.* **2013**, *135*, 9267.

[3] Q. Liu, J. Tian, W. Cui, P. Jiang, N. Cheng, A. M. Asiri, X. Sun, *Angew. Chem. Int. Ed.* **2014**, *53*, 6710.

[4] Y. Li, H. Wang, L. Xie, Y. Liang, G. Hong, H. Dai, *J. Am. Chem. Soc.* **2011**, *133*, 7296.

[5] S. Xu, D. Li, P. Wu, *Adv. Funct. Mater.* **2015**, *25*, 1127.

[6] D.-Y. Wang, M. Gong, H.-L. Chou, C.-J. Pan, H.-A. Chen, Y. Wu, M.-C. Lin, M. Guan, J. Yang, C.-W. Chen, Y.-L. Wang, B.-J. Hwang, C.-C. Chen, H. Dai, *J. Am. Chem. Soc.* **2015**, *137*, 1587.

[7] X. Jia, Y. Zhao, G. Chen, L. Shang, R. Shi, X. Kang, G. I. N. Waterhouse, L.-Z. Wu, C.-H. Tung, T. Zhang, *Adv. Energy Mater.* **2016**, 1502585.

[8] X. Wang, Y. V. Kolen'ko, X.-Q. Bao, K. Kovnir, L. Liu, *Angew. Chem. Int. Ed.* **2015**, *54*, 8188.

[9] H. Yan, C. Tian, L. Wang, A. Wu, M. Meng, L. Zhao, H. Fu, *Angew. Chem. Int. Ed.* **2015**, *127*, 6423.

[10] Z. Huang, C. Lv, Z. Chen, Z. Chen, F. Tian, C. Zhang, *Nano Energy* **2015**, *12*, 666.

[11] H. B. Wu, B. Y. Xia, L. Yu, X.-Y. Yu, X. W. D. Lou, *Nat. Commun.* **2015**, *6*, 6512.

[12] X.-Y. Yu, L. Yu, H. B. Wu, X. W. Lou, *Angew. Chem. Int. Ed.* **2015**, *54*, 5331.

[13] Y. Yang, H. Fei, G. Ruan, J. M. Tour, *Adv. Mater.* **2015**, *27*, 3175.

[14] H. Yin, S. Zhao, K. Zhao, A. Muqsit, H. Tang, L. Chang, H. Zhao, Y. Gao, Z. Tang, *Nat. Commun.* **2015**, *6*, 6430.

[15] L. Yu, B. Y. Xia, X. Wang, X. W. Lou, *Adv. Mater.* **2016**, *28*, 92.

[16] X. Zou, X. Huang, A. Goswami, R. Silva, B. R. Sathe, E. Mikmekova, T. Asefa, *Angew. Chem. Int. Ed.* **2014**, *53*, 4372.

[17] X. Zheng, J. Xu, K. Yan, H. Wang, Z. Wang, S. Yang, *Chem. Mater.* **2014**, *26*, 2344.

[18] J. Tian, Q. Liu, N. Cheng, A. M. Asiri, X. Sun, *Angew. Chem. Int. Ed.* **2014**, *53*, 9577.

[19] P. C. K. Vesborg, B. Seger, I. Chorkendorff, *J. Phys. Chem. Lett* **2015**, *6*, 951.

[20] X. Zou, Y. Zhang, *Chem. Soc. Rev.* **2015**, *44*, 5148.